Magnetic Resonance in Radiotherapy

Supriyanto Ardjo Pawiro

The British Journal of Radiology, 79 (2006), S16–S26

Applications of magnetic resonance spectroscopy in radiotherapy treatment planning

G S PAYNE, DPhil and M O LEACH, PhD, FInstP, FMedSci

Cancer Research UK Clinical Magnetic Resonance Research Group, Institute of Cancer Research and Royal Marsden NHS Trust, Downs Road, Sutton, Surrey SM2 5PT, UK

ABSTRACT. Following advances in conformal radiotherapy, a key problem now facing radiation oncologists is target definition. While MRI and CT provide images of excellent spatial resolution, they do not always provide sufficient contrast to identify tumour extent or to identify regions of high cellular activity that might be targeted with boost doses. Magnetic resonance spectroscopy (MRS) is an alternative approach that holds great promise for aiding target definition for radiotherapy treatment planning, and for evaluation of response and recurrence. MRS is able to detect signals from low

Introduction

- Magnetic resonance spectroscopy is a non invasive technique for measuring biochemical in tissue.
- The advantage of MRS produce signals at different frequencies, depending on the bonding to neighboring nuclei.

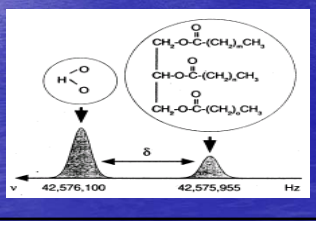

Magnetic Nuclei studied

- MRS ^{1}H is the most sensitive magnetic nucleus and hydrogen is present in nearly all biologically relevant compound.
- For comparison of spectra it is necessary to have a reference frequency
- For consistency, the position of spectral peak in vivo expressed relative to tetrametylsilane (TMS) even though it is not present in tissue.
- Other nuclei that may procedure useful MR spectra are ^{31}P, ^{13}C, and ^{19}F.

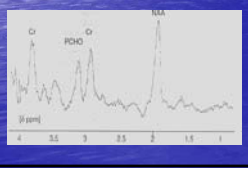

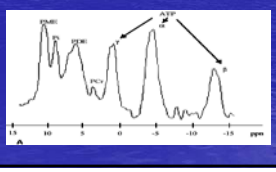

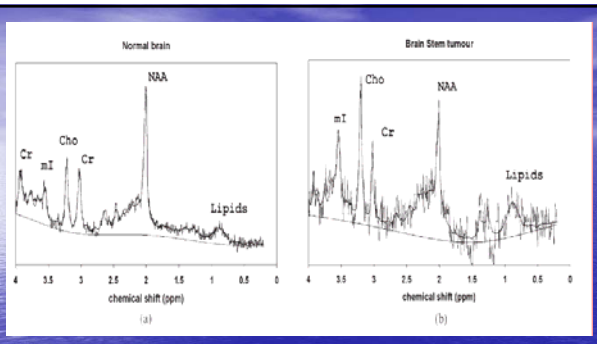

Figure 1. Example of ^{1}H MRS spectra from (a) normal brain and (b) brain stem tumour. The major peaks are from choline (Cho), Creatine (Cr), myo-Inositol (mI), N-acetyl aspartate (NAA) and lipids (lip). Repetition time (TR)=1.5 s; echo time (TE)=30 ms. Each spectrum shows acquired data (grey line), the fit (bold line) and fitted baseline. Note the increase in choline (Cho) and reduction in NAA in the tumour compared with normal brain.

Table 1. Brief details of some metabolites seen in ^{1}H spectra of tissues

Metabolite	Chemical shift of main peak (ppm)	Number of equivalent ^{1}H nuclei	Multiplicity	Description
Cho	3.2	9	singlet	"Cho" includes contributions from choline, phosphocholine, glycerophosphocholine and other trimethylamines. These metabolites are involved in cell membrane lipid synthesis and breakdown, and are also affected by signalling pathways that can be upregulated in tumours. Since 9 magnetically-equivalent protons contribute to this peak, relatively low concentrations produce a measurable signal
Cr	3.02	3	singlets	"Cr" includes creatine and phosphocreatine, which are both involved in energy metabolism
	3.9	2		
Lactate	1.33	2	doublet	Lactate is a product of anaerobic glycolysis, a further aspect of energy metabolism, often being found in necrotic areas
Lipids	1.3, 0.9 etc.		singlet	Often found in necrotic regions
myo-Inositol (mI)	3.52	2	doublet of doublets	This can be detected in brain using shorter echo time acquisitions. Understood to be an essential ingredient for cell growth, an osmolite, and a storage form of glucose
	3.6	2	triplet	
NAA	2.01	3	singlet	NAA is considered to be a neuronal marker, so only present in brain
Citrate	2.6	1	multiplet	This is synthesized and accumulated by normal prostate epithelial tissue

Localization strategy and Validation

- MRS localization techniques fall into two groups. Single-voxel methods include those known as PRESS/STEAM/ISIS in which data are required from a single voxel positioned using MR images.
- The alternative is MRSI as known as chemical shift imaging (CSI) in which a matrix of spectra are acquired either over a plane (2D-MRSI) or a volume (3D-MRSI).
- Registration MR- CT images and motion issues
- Before radiation oncologist have the confidence to alter treatment plans based on MRS data, they need evidence that the abnormality detected using MRS represents tumor.
- The gold standard for comparison is histopathology

Table 2. Comparison of single voxel techniques with spectroscopic imaging

	Single voxel	Spectroscopic imaging
1. *Specification of VOI*		
No. of volumes	1	Typically 8 × 8 × 8 (3d) or 16 × 16 (2d)
Voxel specification	Must be specified before measurement	Many voxels available Grid shift can be performed retrospectively
Voxel shape	Dimensions adjustable; also tilt	Orthogonal (usually square) grid
2. *Voxel integrity*		
Edge definition	That of slice profile	Point spread function effects
Chemical shift displacement artefact	Yes – in each direction	Not present
3. *Sensitivity*		
Relaxation losses	T_2 (STEAM, PRESS)	T_2 (in STEAM and PRESS pre-localized implementations)
Other losses	Imperfect RF pulse profiles and flip angles	Phase-encoding loses approximately 13% in each spatial dimension
Conformation to target	Usually good	Sometimes poor. Addition of small voxels does not recover SNR of the larger corresponding voxel
4. *Other aspects*		
Minimum number of acquisitions	1	Many (e.g. 512 for 8 × 8 × 8 csi)
RF coils – uniform transmit coils and surface coil receiver	Good	Good
RF coils – transmit/receive surface coil	ISIS works well provided adiabatic RF pulses are used; PRESS and STEAM rely on slice selection which is not good with the non-uniform transmit fields from surface coils	The basic implementation works well if an adiabatic excitation pulse is used; additional localization (slice or volume selection) have same problems as PRESS and STEAM

VOI, volume of interest; RF, radiofrequency; SNR, signal to noise ratio.

Case 1: MRS and Brain cancer

- There is a strong incentive for non-invasive assessment of brain cancer, particularly for children.
- MRI appearance and localization alone have limited power to differentiate brain tumor, particularly early stage disease and infiltrative disease
- ^{1}H MRS of brain tumors has developed rapidly due to the less technical requirements of spectroscopy in the brain compared with measurements elsewhere in the body.

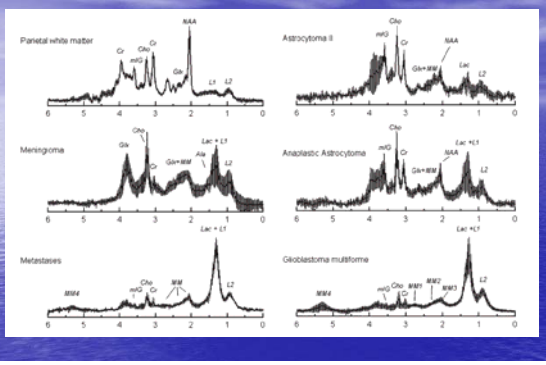

Figure 2. Mean and standard deviation (vertical lines) of normalized STEAM (echo time (TE)=30 ms) spectra acquired from a number of subjects: Normal white matter (n=6); meningioma (n=8); astrocytoma grade II (n=5); anaplastic astrocytoma (n=7); glioblastoma (n=13). Published with permission [28].

Table 3. Summary of ^{1}H MRS characteristics of different brain tumours

Tumour type	^{1}H MRS characteristics
All tumour types	Low NAA, and reduced Cr
Astrocytomas	Elevated Cho, reduced Cre and significantly reduced NAA. With increasing WHO grade, methylene lipid (1.3) and lactate may be seen, indicating necrosis. Methylene levels correlate with contrast enhancement in MR images, and may allow the transformation from low to high grade to be detected prior to focal contrast enhancement [63]. Cho may also increase with the increased proliferative activity of higher grade tumours. Glioblastoma multiforme has the same spectral pattern as metastasis
Low grade tumours	May show increased mI
Oligodendoglioma and mixed oligoastrocytoma	mI may also be elevated, together with Cho
Meningioma	Low [Cr] and [mIG], increased Cho, although there may be low levels of lipids and a characteristic presence of alanine (1.47)
Metastasis	Similar features to astrocytomas, with increased lipid if necrosis is present. However, they may have a distinct spectroscopic boundary. Thus the presence of elevated choline/creatine ratio in the peritumoural region may suggest high grade glioma rather than a solitary metastasis [64]
Radiation necrosis	In some cases produces a peak at 2.4 ppm [65]

- Recently there has been increasing interest in using functional imaging techniques, together with metabolic imaging using MRS to aid target definition in radiotherapy.
- Area of relatively high Cho/NAA may indicate high cellular activity, and hence radio-sensitivity, and Lac may indicate hypoxic area with reduces radiosensitivity.
- The technique can also be helpful in identifying area missed by radiation fields, and in separating recurrence from radiation necrosis.
- Reduction in Cho and Lipid and lactate can also reflect response to chemotherapy and radiotherapy.

Therapeutic guidance, assessment of response and recent development

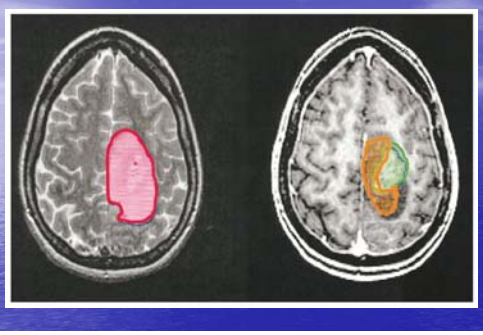

Figure 3. Comparison of lesion extent measured using T_2 weighted MRI (red), T_1 weighted MRI following injection of contrast agent (green), and MRS to measure high Cho/NAA (orange) for a patient with a grade 4 glioma. Published with permission [43].

- MRS has been compared with MRI and SPECT in monitoring response to treatment in metastasis brain tumor.
- Reduction in Cho and Lac and increasing Lip (believe to represent necrosis) in corresponding tumor were detected at earlier time (1 week to 1 months) than contrast enhanced MRI or SPECT.

Case2 : MRS and Prostate

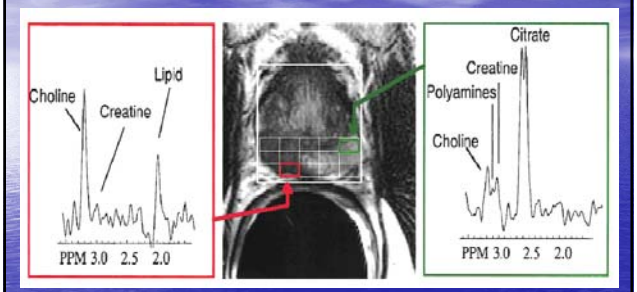

Figure 4. Centre: T_2 weighted transverse image of prostate with tumour in right mid-gland, overlain with grid of voxels from which spectra were acquired. Left: Spectrum acquired from region of tumour, illustrating dramatically elevated choline and absence of citrate and polyamines. Right: Spectrum from healthy peripheral zone tissue with high citrate and presence of polyamines. (Reproduced with permission from J Kurhanewicz et al [46]).

Validation

- A strong correlation has been found between negative MRSI and negative biopsy findings, and between positive MRSI and positive biopsy findings
- There is only a weak correlation between the concentration of prostate specific antigen (PSA, the current "gold standard") and either biopsy or MRSI findings
- Several studies have shown that adding MRSI to an MRI examination increases the accuracy of diagnosis

Recurrence

- Use of MRSI together with MRI has been shown to improve substantially the identification of tumor recurrence following external beam radiotherapy (the area under the ROC curve, a measure of the effectiveness of a test, increased from 0.5 to 0.81
- The presence of 3 or more suspicious voxels in a hemiprostate showed a sensitivity and specificity of 89% and 82%, respectively, for the diagnosis of local recurrence

Planning

- MRSI has been used in combination with MRI to define regions for dose escalation within the prostate, permitting a dose of > 90 Gy to the high-risk region while treating the remainder of the prostate to about 70 Gy

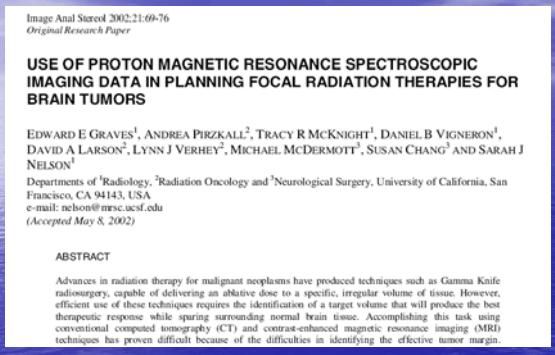

Image Anal Stereol 2002;21:69-76
Original Research Paper

USE OF PROTON MAGNETIC RESONANCE SPECTROSCOPIC IMAGING DATA IN PLANNING FOCAL RADIATION THERAPIES FOR BRAIN TUMORS

EDWARD E GRAVES[1], ANDREA PIRZKALL[2], TRACY R MCKNIGHT[1], DANIEL B VIGNERON[3], DAVID A LARSON[2], LYNN J VERHEY[2], MICHAEL MCDERMOTT[3], SUSAN CHANG[3] AND SARAH J NELSON[1]

Departments of [1]Radiology, [2]Radiation Oncology and [3]Neurological Surgery, University of California, San Francisco, CA 94143, USA
e-mail: nelson@mrsc.ucsf.edu
(Accepted May 8, 2002)

ABSTRACT

Advances in radiation therapy for malignant neoplasms have produced techniques such as Gamma Knife radiosurgery, capable of delivering an ablative dose to a specific, irregular volume of tissue. However, efficient use of these techniques requires the identification of a target volume that will produce the best therapeutic response while sparing surrounding normal brain tissue. Accomplishing this task using conventional computed tomography (CT) and contrast-enhanced magnetic resonance imaging (MRI) techniques has proven difficult because of the difficulties in identifying the effective tumor margin.

Gamma Knife Radiosurgery planning and delivery

- At University California San Francisco, the clinically utilized radiological unit is the gamma knife from Elekta instrument
- The morning of treatment, a stereotactic frame is attached to patient's skull to provide a means of immobilization as well as a coordinate reference system
- The patient then undergoes an MR examination which is subsequently transferred to a workstation for treatment planning using GammaPlan software.

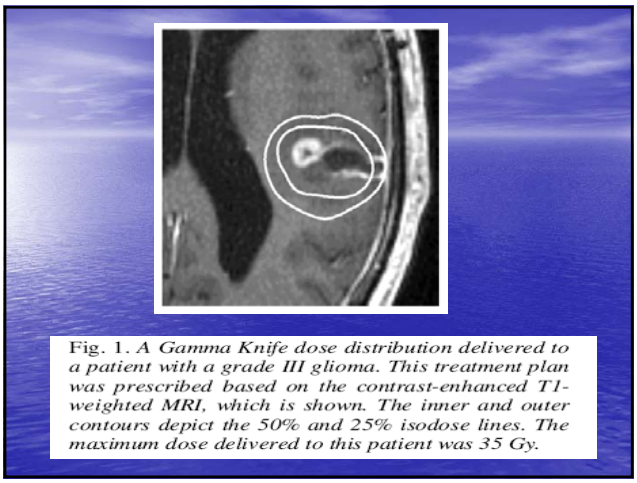

Fig. 1. *A Gamma Knife dose distribution delivered to a patient with a grade III glioma. This treatment plan was prescribed based on the contrast-enhanced T1-weighted MRI, which is shown. The inner and outer contours depict the 50% and 25% isodose lines. The maximum dose delivered to this patient was 35 Gy.*

Acquisition of MRSI Data

- Three dimensional MRSI acquisition employing a point resolved spectroscopy (PRESS) technique.
- A phase encoding matrix of 8x8x8, 16x8x8, or 12x12x8 chosen based on the dimensions of the volume to be excited.
- All MRSI acquisitions use a TR of 1000 ms, TE of 144 ms, and are acquired in 17 – 19 minutes

Reconstruction of MRSI Data

- Reconstruction and analysis of 3D MRSI data is achieved by transferring the data from the scanner to an offline UltraSPARC solaris workstation.
- The peak parameters (height, area, and width) for choline, creatine (Cr), N-acetyl aspartate (NAA), and lactate/lipid (LL) are then calculated for each voxel
- Statistical routine has been developed that computes a measure of abnormality for each spectral voxel in dataset based on the extent to which its choline and NAA levels.
- The measurements is referred to as the choline/NAA residual, and has been shown to reproducibly quantity the degree of spectral abnormality in voxel relative to normal voxel.

Correlation of MRSI with Treatment planning MRI

- Registration of the MRI component of MRSi examination to MRI dataset being used for GK treatment planning
- The choline/NAA residual map determined from the registered MRSi data is then resampled to the resolution of the registered MRI, and represented as contour map at levels of 2.0, 3.0, and 4.0
- The contour are represented within the registered MRI pixel data and the final image is sent to TPS.
- The same coordinate frame as planning image dataset and spectral contour can be used to guide the delineation of radiation target.
- This technique was been shown to reproducibility identify the region of spectroscopic abnormality in glioma patients within 3 mm.

Differences between anatomic and metabolic lesions in brain tumors

- The authors have review more than 1500 combined MRI/MRSi examinations of patens with brain tumors
- 100 patients with recurrent primary brain tumors, 36% of patients with high grade lesion and 50% of patient with mid or low grade lesions had spectra with elevated choline and decreased NAA outside the region of contrast enhancement
- Only 50% of the T2 hyperintense region had voxel with a choline/NAA residual greater that or equal 2.0
- This phenomena useful for both expanding high dose treatment volume beyond the contrast enhancing region and limiting the dose delivered
- If T2 hyperintense regions with choline/NAA residual value greater than 2.0, 3.0, and 4.0 in population of patient with newly diagnosed grade III and grade IV glioma

Implications of Metabolic target delineation for gamma knife radiosurgey

- The pre-treatment metabolic lesion of 36 glioma patient undergoing gamma knife radiosurgey were compared to the radiation target volume and to patients clinical outcome.
- The result of this analysis demonstrated a tendency for poorer responses, in terms of survival time, time to further treatment, and change in contrast enhancing volume, among patients with spectroscopic abnormalities that extended beyond the target volume at the time of treatment

- The gamma knife radiosurgery is focal ablative therapy, modification of the prescribed radiation target based on MRSI data has proceeded cautiously
- Its is important that the target only have diameter less or equal to 4 cm can be effectively treated with radiosurgery
- The constructed plan is then viewed superimposed on the choline/NAA residual contour labeled MRI image within Gamaplan
- In situation where the extent of abnormal spectroscopic voxels is larger than the maximum permissible volume for radiosurgery, the strategy suggest target the use of concurrent chemotherapy

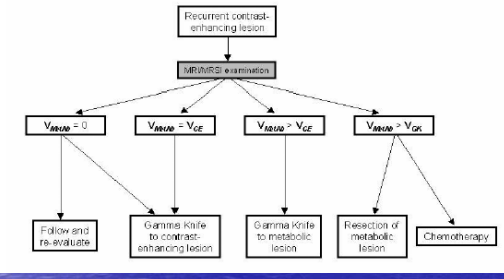

Fig. 4. *A flowchart depicting a possible treatment selection and planning strategy that incorporates MRSI findings. The final nodes for each path depict possible courses of action in the treatment of brain tumor patients displaying the corresponding diagnostic features. V_{MetAb}: volume of the metabolic abnormality as determined by MRSI, V_{CE}: volume of contrast enhancement, V_{GK}: maximum permissible Gamma Knife target volume.*

Differentiation Between Brain Tumor Recurrence and Radiation Injury Using MR Spectroscopy

Patrick Weybright[1]
Pia C. Sundgren[1]
Pavel Maly[1]
Diana Gomez Hassan[1]
Bin Nan[2]
Suzan Rohrer[1]
Larry Junck[3]

OBJECTIVE. The purpose of our study was to explore the feasibility and utility of 2D chemical shift imaging (CSI) MR spectroscopy in the evaluation of new areas of contrast enhancement at the site of a previously treated brain neoplasm.

MATERIALS AND METHODS. Two-dimensional CSI (point-resolved spectroscopy sequence [PRESS]; TR/TE, 1,500/144) was performed in 29 consecutive patients (4–54 years old; mean age, 34 years) who had a new contrast-enhancing lesion in the vicinity of a previously diagnosed and treated brain neoplasm. Clinical and imaging follow-up, and histopathology in 16 patients, were used as indicators of the identity of a lesion.

RESULTS. Diagnostic-quality spectra were obtained in 97% of the patients. The Cho/Cr (choline/creatine) and Cho/NAA (choline/*N*-acetyl aspartate) ratios were significantly higher, and the NAA/Cr ratios significantly lower, in tumor than in radiation injury (all three differences, $p < 0.0001$). The Cho/Cr and Cho/NAA ratios were significantly higher in radiation injury than in normal-appearing white matter ($p < 0.0003$ and $p < 0.0001$, respectively), whereas NAA/Cr ratios were not different ($p = 0.075$). Mean Cho/Cr ratios were 2.52 for tumor, 1.57 for radiation injury, and 1.14 for normal-appearing white matter. Mean Cho/NAA ratios were 3.48, 1.31, 0.79, and mean NAA/Cr ratios were 0.79, 1.22, and 1.38, respectively. When values greater than 1.8 for either Cho/Cr or Cho/NAA ratios were considered evidence of tumor, 27 of 28 patients could be correctly classified.

CONCLUSION. Two-dimensional CSI MR spectroscopy can differentiate tumor from radiation injury in patients with recurrent contrast-enhancing intracranial lesions. In these lesions, the Cho/NAA and Cho/Cr ratios may be the best numeric discriminators.

Subject:

- 29 patient (16 male, 13 female), 4- 54 year
- All patient got fractionated radiation therapy (54 – 70 Gy)
- Tumor stages are II - IV

Methods:

- Successful 2D CSI was performed in 28 of 29 patients.
- The following parameters were used for all 2D CSI examinations: a point-resolved spectroscopy sequence (PRESS); TR/TE, 1,500/144;
- Field of view, 16 cm; matrix, 16 × 16; slice thickness, 10–20 mm; acquisition, 1 average; scanning time, 4 min 20 sec

Analysis:

- The spectra were analyzed for the signal intensity of NAA, choline, and creatine and for the presence of lactates and lipids.
- Ratios were manually calculated for NAA/Cr, Cho/Cr, and Cho/NAA
- Metabolite ratios among the recurrent tumor population and radiation injury population were compared.
- The highest Cho/Cr, Cho/NAA, and NAA/Cr ratios in one voxel were used for comparison
- Two locations in the brain of 26 of 28 patients were measured, one in the contrast-enhancing lesion and one in the normal-appearing white matter.
- The generalized estimating equation technique was used to fit a linear regression model for each of the three ratios to take into account the within-subject correlation
- Robust SEs were used to compute Wald test *p* values. The level for statistical significance was set to a *p* value of less than 0.05
- The reference is histopathology

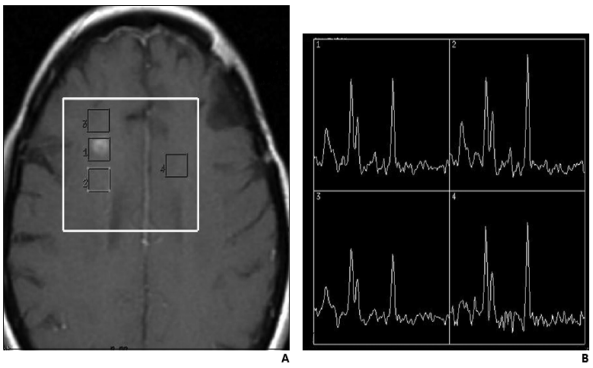

Fig. 1—43-year-old woman after surgical resection, radiation, and chemotherapy for left frontal anaplastic oligodendroglioma.
A, Axial T1-weighted image after contrast administration shows focal new area of contrast enhancement in right frontal lobe on 2D chemical shift imaging MR spectroscopy with volume of interest placed over lesion.
B, Spectra show mild alterations in metabolic peaks, with slightly increased Cho/Cr (choline–creatine) ratio (1.76), slightly increased Cho/NAA (choline–*N*-acetyl aspartate) ratio (1.19), and normal NAA/Cr ratio (1.48), indicating mild elevation of choline peak. Interval follow-up showed complete resolution of contrast-enhancing lesion without any additional treatment, supporting diagnosis of radiation injury.

TABLE 1: Ratios Between Choline, Creatine, and NAA in Recurrent Tumor, Radiation Injury, and Normal-Appearing White Matter

Ratio	Tumor (16 patients)	Radiation Injury (12 patients)	Normal-Appearing White Matter (26 patients)
Cho/Cr	2.52 (1.66–4.26)	1.57 (0.72–1.76)	1.14 (0.86–1.59)
Cho/NAA	3.48 (1.70–6.47)	1.31 (0.83–1.78)	0.79 (0.56–1.2)
NAA/Cr	0.79 (0.47–1.15)	1.22 (0.94–1.69)	1.39 (0.64–2.0)

Note—Data are mean ratios (ranges in parentheses). Cho = choline, Cr = creatine, NAA = *N*-acetyl aspartate.

- Tumor had significantly higher Cho/Cr than the radiation injury and had significantly higher Cho/Cr ratios than the normal-appearing white matter
- The lesions in the tumor group also had significantly higher Cho/NAA ratios than those in the radiation injury group and lesions in this group again had significantly higher Cho/NAA ratios than the normal-appearing white matter
- Lesions in the tumor group had significantly lower NAA/Cr ratios than those in the radiation injury group, which had insignificantly lower NAA/Cr ratios than the normal-appearing white matter

TABLE 2: Borderline Ratios: Overlap in Either Cho/Cr or Cho/NAA Ratios Between Patients with Tumor or Radiation Injury—Four Patients from Each Group

Tumor	Radiation Injury
Cho/Cr: 1.66 (Cho/NAA: 1.34)[a]	Cho/Cr: 1.76 (Cho/NAA: 1.11)
Cho/Cr: 1.69 (Cho/NAA: 3.07)	Cho/Cr: 1.70 (Cho/NAA: 1.01)
Cho/Cr: 1.74 (Cho/NAA: 2.00)	Cho/NAA: 1.78 (Cho/Cr: 1.64)[b]
Cho/NAA: 1.70 (Cho/Cr: 1.96)	Cho/NAA: 1.71 (Cho/Cr: 1.61)[b]

Note—Cho = choline, Cr= creatine, NAA = *N*-acetyl aspartate.
[a]Probably from nonneoplastic portion of lesion. The only tumor patient with both ratios lower than 1.8.
[b]Both contrast-enhancing (posterior fossa) lesions proved negative for tumor at biopsy and resolved with time.

- None of the lesions classified as radiation injury reached the value of 1.8 in either Cho/Cr or Cho/NAA ratios. Two lesions classified as radiation injury had Cho/NAA ratios of 1.71 and 1.78, respectively.
- Two patients with tumor who had Cho/Cr ratios lower than 1.8 had Cho/NAA ratios higher than 1.8 (3.07 and 2.00). One patient with tumor who had a Cho/NAA ratio less than 1.8 had a Cho/Cr ratio greater than 1.8 (1.96)
- Only one patient with tumor had both Cho/Cr and Cho/NAA ratios lower than 1.8.

Discussion

- Have presented identifying tumor extent and metabolically active regions to aid targeting of radiotherapy, evaluating response to treatment, and identifying recurrence and radiation injury
- The limitation voxel size is typically 8 mm^3 to 10 mm^3 to achieve SNR
- Need improvement of sensitivity and spectral specificity to achieve the good resolution
- For radiotherapy planning, MR doesn't provide electron density

Assessment of geometrical accuracy of magnetic resonance images for radiation therapy of lung cancer

Journal of Applied Clinical Medical Physics 4 (4), 2003

N. Koch, H.H. Liu, L.E. Olsson,
and E.F. Jakson

Introduction

- Interest in the assessment of respiration induced lung tumor motion has increased with advent of gated therapy
- Complementary to x-ray computed tomography, MR imaging offer unique capabilities for tracking the tomor with flexible imaging plane
- They exploited some features of MR imaging using two pulse sequences: a cine imaging sequence designed for tracking lung tumor during respiration.
- Localized fluctuation in the magnetic field originating from large susceptibility difference can cause distortion near air-tissue interfaces

Methods: Theoretical simulation

- Difference in magnetic susceptibility between two materials creates microscopic pertubation in magnetic fields
- In the human body, interfaces of air (x ~0.36 ppm) and tissue (X~ -11 to -7.0 ppm) give rise to the largest natural magnetic susceptibility field pertubation.
- The distortion is also dependent on the shape of the interface or object and the orientation of its axis
- Circular cross sections of vials with this axis oriented perpendicular and parallel with direction of main magnetic field.

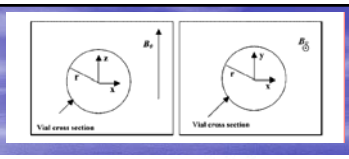

$$\Delta B_z(x,z)=\frac{\Delta\chi B_0 r^2}{2}\frac{z^2-x^2}{(x^2+z^2)^2}, \quad (1)$$

where r is the radius of the vial, z is the distance from the vial center in the z direction, and x is the distance from the vial center in the x direction.[2] ΔB_z inside the vial is given as

$$\Delta B_z=\frac{\Delta\chi B_0}{2}. \quad (2)$$

For situation 2, Eqs. (1) and (2) reduce to $\Delta B_z=\Delta\chi\, B_0$ and $\Delta B_z=0$, respectively. The positional error created by ΔB_z is simply ΔB_z divided by the readout gradient magnitude G_r, which is

$$G_r=\frac{BW}{\gamma FOV}, \quad (3)$$

where BW is the bandwidth, γ is the gyromagnetic ratio, and FOV is the field-of-view. Thus, the position error can be calculated as,

$$x'(x,z)=x+\frac{\Delta B_z(x,z)}{G_r}. \quad (4)$$

Methods: Phantom experiments

- Phantom was designed and built in house to approximate the geometry of the upper thorax, including two air cavities that served as simulated lung
- The phantom size was 35 x 41 x 17 cm^3 with cavity of the phantom measured 28 x 15 x 15 cm^3 and contained the inserts.
- The inserts were designed to hold vial in place so vial cross-sections could be imaged in the sagital and coronal planes.

- The inner diameter of the vials was about 1.5 cm and the distance between two adjacent vial was approximately of 3.8 – 5.6 cm depending on the arrangement.
- The filling phantom and vials, except the air cavities was 8.3 L of a solution consisting of deinonized water, 2.4 gram/L NaCl, 18 mL Gd-DTPA doping agent. The solution has a measured T1/T2 of 204/112 ms
- MR images were acquired of phantom on a 1.5 T whole body signal echo speed MR scanner and an fGRE sequence was used to get images with parameters : BW 83.3 kHz, FOV=44 cm, TE/TR = 2/4 ms, flip angle 60º, NEX = 3.0, matrix = 512 x 512 and slice thickness 1.0 mm.
- Second sequence fast spin echo (FSE) was used to get images with parameters : BW 62.5 kHz, FOV=44 cm, TE/TR = 9.4/600 ms, echo train length=3, NEX = 3.0, and matrix = 512 x 512

Analysis

To register an MR image with its corresponding CT image, a new coordinate system common to both the images was defined. This was accomplished by first choosing a registration point from the COM of one of the vials as centrally located in the image as possible. This registration point subsequently became the origin of the common coordinate frame. (See Fig. 7) Next, using the least squares method, a common x axis was fit through a row of vial centroids including the registration point. The y axis was set perpendicular to the x axis and passed through the registration point. The rotation angle of the object in the image was determined from the slope of the common x axis using, i.e., $\theta = \arctan(m_0)$, where m_0 is the slope of the fit x axis to the object. Then, a matrix transformation registered the COM coordinates in their original Cartesian image frame to the common coordinate frame,

$$[x' \; y' \; 1] = [x \; y \; 1] * \begin{bmatrix} \cos(\theta) & \sin(\theta) & 0 \\ -\sin(\theta) & \cos(\theta) & 0 \\ 0 & 0 & 1 \end{bmatrix} \frac{FOV}{MATRIX}, \qquad (6)$$

where *(FOV/MATRIX)* scales the object coordinates to centimeters.

With the COM coordinates computed in their new registered frame, each vial centroid position in the MR and CT images was compared. The differences in the coordinates along the PE and FE directions were compiled separately for each image set. However, the displacement in the FE direction caused by susceptibility differences cancels out when the vials in the respective images

Result

A. Theoretical simulation

The positional shift in the FE direction created by susceptibility differences between the whole blood and air is illustrated in Fig. 5. This figure illustrates the case where the blood vessels are parallel to the magnetic field, as the circular cross-sections of vessels would be during axial image acquisition. Here, $\Delta B_z = \Delta\chi \; B_0$ and $\Delta B_z = 0$, are used in Eqs. (3) and (4) with the parameters $B_0 = 1.5$ T, $\Delta\chi = -7.90$, BW = 62.5 kHz, FOV = 44 cm, and $\gamma = 42.58$ MHz/T. The theoretical maximum displacement due to susceptibility differences alone is −3.7 mm.

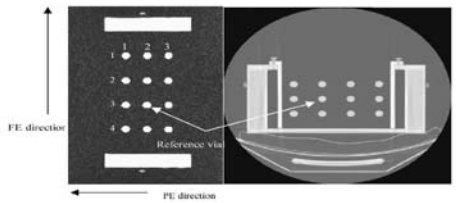

FIG. 7. A CT image (at left) and a sagittal MR image (at right) of the phantom. The directions of the PE and FE, the index for the columns, and rows of the vials are shown.

Figure 6 shows the shift when the vial axes are perpendicular to the magnetic field, as they were during coronal and sagittal image acquisition. Here, the results of Eqs. (1)–(4) are combined with the parameters $B_0 = 1.5$ T, $\Delta\chi = -7.90$, $r = 1.5$ cm, BW = 83.3 kHz, FOV = 44 cm, and $\gamma = 42.58$ MHz/T to generate this figure. The theoretically largest displacement is 1.4 mm.

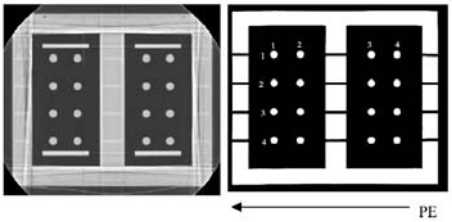

FIG. 8. A CT image (at left) and a coronal MR image (at right) of the phantom. The results in Table III are arranged to correspond with the row and column indices shown in the MR image.

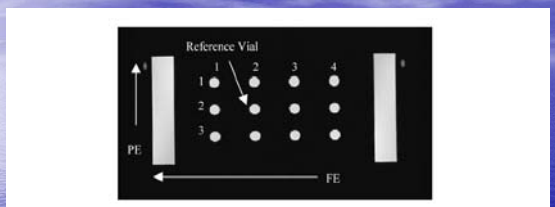

FIG. 9. An axial MR image of the phantom. The corresponding CT image is similar to that shown in Fig. 7. The reference vial, PE and FE directions, and column and row indices are labeled.

Sagital of 1st sequence

Coronal

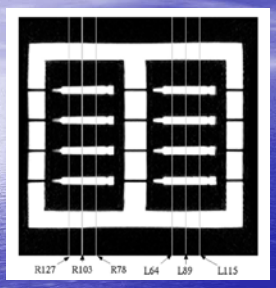

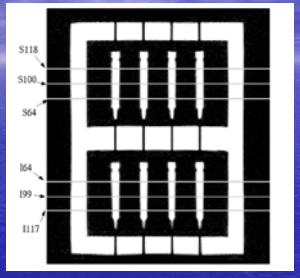

To measure the accuracy, the result compare standard from CT images

TABLE I. The average absolute differences in vial positions from the sagittal fGRE MR images in the two most lateral slices (R127 and L115, see Fig. 3).

	Direction	Column 1 avg (mm)	Column 2 avg (mm)	Column 3 avg (mm)
Row 1	FE	0.6	0.4	0.2
	PE	0.6	0.7	0.5
Row 2	FE	0.4	0.3	0.4
	PE	0.3	0.3	0.6
Row 3	FE	0.1	0.0	0.1
	PE	0.1	0.0	0.4
Row 4	FE	0.8	0.3	0.3
	PE	0.5	0.1	0.3

TABLE II. The average absolute differences in vial positions from the sagittal fGRE MR images in the two most medial slices (R78 and L64, see Fig. 3).

	Direction	Column 1 avg (mm)	Column 2 avg (mm)	Column 3 avg (mm)
Row 1	FE	0.4	0.3	0.2
	PE	0.3	0.4	0.4
Row 2	FE	0.2	0.2	0.3
	PE	0.3	0.2	0.4
Row 3	FE	0.2	0.0	0.1
	PE	0.3	0.0	0.2
Row 4	FE	0.7	0.4	0.2
	PE	0.5	0.1	0.1

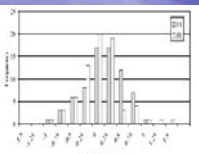

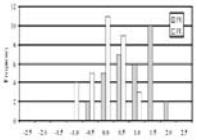

TABLE III. The average absolute differences in the vial positions from the two coronal slices (see Fig. 7).

	Direction	Column 1 avg (mm)	Column 2 avg (mm)	Column 3 avg (mm)	Column 3 avg (mm)
Row 1	FE	1.4	1.3	0.6	0.3
	PE	0.6	0.4	1.0	1.2
Row 2	FE	1.4	1.2	0.2	0.1
	PE	0.4	0.3	0.4	0.6
Row 3	FE	0.9	1.3	0.0	0.0
	PE	0.4	0.3	0.0	0.1
Row 4	FE	1.3	1.0	0.2	0.7
	PE	0.5	0.5	0.4	0.3

TABLE IV. The average absolute differences in the vial positions in the most medial axial slices (see Fig. 8).

	Direction	Column 1 avg (mm)	Column 2 avg (mm)	Column 3 avg (mm)	Column 4 avg (mm)
Row 1	FE	0.6	1.0	1.5	2.1
	PE	1.9	0.3	1.1	2.6
Row 2	FE	0.3	0.0	0.5	1.0
	PE	1.5	0.0	1.5	3.0
Row 3	FE	1.3	1.0	0.3	0.3
	PE	1.2	0.3	1.9	3.5

For the axial FSE images, Table IV shows the differences in the vial positions averaged for the two medial axial slices. Notice that all of the vials except those in column 4 of Table IV, showed average absolute differences within 2.0 mm in the PE and FE directions (1.7 ± 1.0 mm and 0.9 ± 0.6 mm, respectively). Results of the two other pairs of mid-cavity and outermost slices showed increased differences. Table V shows the outermost slices. Large differences are seen at the corner vial locations. The averaged absolute differences for all locations in the PE and FE directions were 1.7 ± 1.0 mm and 1.2 ± 0.7 mm, respectively. The maximum difference was 3.6 mm in the PE direction for a vial at row 1 and column 1 situated at the corner in an innermost slice. The results indicated that the differences along the PE direction showed no apparent dependency on imaging plane or vial location. However, the differences in the FE direction decreased for the vials closer to the magnet's center.

TABLE V. The average absolute differences in the vial positions in the most distal and proximal axial slices (see Fig. 8).

	Direction	Column 1 avg (mm)	Column 2 avg (mm)	Column 3 avg (mm)	Column 4 avg (mm)
Row 1	FE	1.0	1.1	1.6	2.5
	PE	1.9	0.4	0.9	2.3
Row 2	FE	0.9	0.0	0.6	1.4
	PE	1.4	0.0	1.4	2.9
Row 3	FE	1.3	1.0	0.6	0.8
	PE	1.2	0.5	2.1	3.4

- In registering the MR and CT images, a common coordinate frame was established with an original selected near the center of image. The rationale of such an approach is that the image distortion is minimum near the center of the magnetic field.
- Though the differences in the vial positions between the MR and CT images could be subject to the specific location of the reference point, we expect that the effect of choosing the reference point would be negligible as long as it is near the center of the magnet and FOV.
- In addition, the position differences measured from the fGRE images were all significantly less than 2 mm.

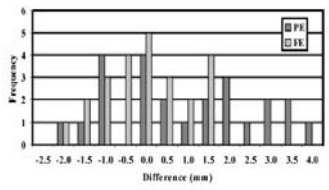

FIG. 12. A histogram showing the frequency of differences that occurred between the positions of vials in axial FSE MR and CT images.

Conclusion

- The vial positions in the sagittal and coronal fGRE images had displacements no greater than 2.0 mm in either the FE or PE direction compared with those from the CT images.
- Discrepancies exceeding the acceptable limit of 2.0 mm were found along the periphery in the axial images using the FSE sequences.
- The spatial accuracy for the sagital and coronal images were found to be acceptable for subsequent patient imaging, whereas additional assessment for the axial image has to be made to improve their spatial accuracy for radiation therapy applications